EUROfusion

EUROFUSION CP(15)07/01

P. Rodrigues et al.

Sensitivity of Alpha–Particle–Driven Alfven Eigenmodes to q–profile Variation in ITER Scenarios

14th IAEA Technical Meeting on Energetic Particles in Magnetic Confinement Systems
Vienna, Austria
(1st September 2015 – 4th September 2015)

This work has been carried out within the framework of the EUROfusion Consortium and has received funding from the Euratom research and training programme 2014-2018 under grant agreement No 633053. The views and opinions expressed herein do not necessarily reflect those of the European Commission.

Sensitivity of alpha-particle–driven Alfvén eigenmodes to q-profile variation in ITER scenarios

P. Rodrigues[1], A. Figueiredo[1], L. Fazendeiro[1], J. Ferreira[1], R. Coelho[1], F. Nabais[1], D. Borba[1], N. F. Loureiro[1], A. Polevoi[2], S. D. Pinches[2] and S. E. Sharapov[3]

[1]Instituto de Plasmas e Fusão Nuclear, Instituto Superior Técnico, Universidade de Lisboa, 1049-001 Lisboa, Portugal.
[2]ITER Organization, Route de Vinon-sur-Verdon, CS 90 046, 13067 St Paul-lez-Durance Cedex, France.
[3]CCFE, Culham Science Centre, Abingdon OX14 3DB, United Kingdom.

Corresponding Author: par@ipfn.ist.utl.pt

Abstract:
A systematic approach to stability assessment of alpha-particle–driven Alfvén eigenmodes in burning plasmas is used to show that ITER $I_\mathrm{p} = 15$ MA baseline scenario is highly sensitive to small changes in the background magnetic equilibrium. Slight perturbations in the total plasma current are seen to cause large variations in the growth rate of the most unstable eigenmodes found. The observed sensitivity is shown to proceed from the very low magnetic shear values attained throughout the plasma core.

1 Introduction

Plasma heating during the burning regime in tokamak reactors will rely upon the energy of fusion-born alpha-particles which must be kept confined to keep the plasma hot and prevent wall damage [1]. However, such particles can drive Alfvén Eigenmodes (AEs) unstable and be thus transported away from the plasma core, which would hamper the burning process [2, 3]. Therefore, to predict the level of alpha-particle redistribution and loss, the most unstable AEs need to be identified for later analysis with more specialized tools.

During experiment planning and design, such identification task must be performed not only for the intended plasma state (e.g., $Q = 10$ for ITER), but also for a few small perturbations of it. This sensitivity analysis enables one to evaluate if the stability properties of the most unstable AEs identified (frequency, wave number, and growth rate) are robust. Because *ab initio* simulations able to provide a self-consistent solution of the interaction between alpha-particles and the bulk plasma are still computationally expensive, more efficient approaches must be employed for routine stability assessments.

The complex interplay between energetic supra-thermal particles and AEs is still not fully understood and recent research concerning ITER [4, 5, 6] has been focusing on the 15 MA baseline scenario [7]. In this work, an hybrid ideal-MHD–drift-kinetic model and the `ASPACK` [6] suite of codes are used to find how the stability properties of AEs change in response to small variations of the background magnetic-equilibrium profiles. Of particular interest are the net growth rate, wave number, and frequency of the most unstable AEs. These properties are shown to be significantly affected by small changes of the safety-factor profile that result from slight perturbations of the total plasma current. The consequences of these results for stability predictions of alpha-particle–driven AEs in burning plasmas are also discussed.

2 Particle-wave interaction model

Routine stability assessments in burning plasmas can be accomplished with an hybrid MHD–drift-kinetic model of particle-wave interaction [6]. Here, ideal-MHD theory is used to describe the bulk plasma and its particle species (fuel ions, electrons, He ash and other impurities) are assumed to have local-Maxwellian energy distribution functions. The radial dependence of the bulk-species temperature and particle-number density is an input and must be obtained from some transport model. A similar input must also be provided for the density of the diluted fusion alpha-particle population, which is assumed to be isotropic in pitch angle and to follow the slowing-down distribution function

$$f_{\mathrm{sd}}(E) = \left(E^{3/2} + E_{\mathrm{c}}^{3/2}\right)^{-1} \mathrm{erfc}\big[(E - E_0)/\Delta_{\mathrm{E}}\big], \tag{1}$$

where E_{c} is the cross-over energy and Δ_{E} is the energy dispersion around the birth energy E_0 [8]. The response of non-Maxwellian alpha-particles to the ideal-MHD perturbation of the bulk plasma is given by a linearized drift-kinetic equation, valid in the approximation

$$\omega/\Omega_\alpha \sim \left(k_\perp \rho_\alpha\right)^2 \ll 1, \tag{2}$$

with ω the AE frequency whereas Ω_α and ρ_α are the alpha-particle gyro-frequency and gyro-radius. This distribution-function response gives rise to a small complex correction $\delta\omega$ to the frequency ω of marginally stable AEs [9]. The alpha-particle contribution to the AE growth rate is then $\gamma_\alpha = \mathrm{Im}(\delta\omega)$ and a similar procedure for the plasma-bulk species j produces the corresponding Landau-damping contribution γ_j to the wave-particle energy exchange. Disregarding non-ideal effects (e.g., Alfvén continuum damping, radiative damping), which cannot be modeled by the perturbative approach just described, the overall AE growth rate is thus $\gamma_\alpha + \sum_j \gamma_j$.

The `ASPACK` workflow for the stability assessment of a given plasma state is as follows [6]: a magnetic equilibrium is computed by `HELENA` [10] using the kinetic profiles obtained from a transport model and all possible AEs are then found by intensively scanning over a frequency and wave-number range with the ideal-MHD code `MISHKA` [11], while the energy transfer between them and all plasma species is evaluated with the drift-kinetic code `CASTOR-K` [12, 13]. The computational efficiency of the `MISHKA`/`CASTOR-K` pair is the

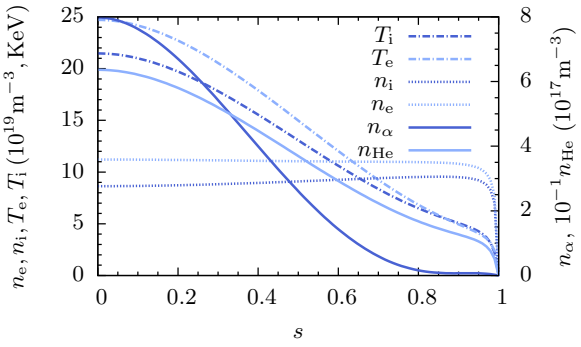

FIG. 1: Radial distribution of the plasma-species densities and temperatures.

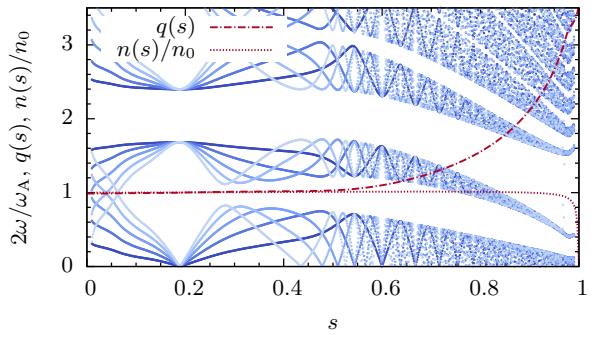

FIG. 2: Ideal Alfvén continuum for $n = 10, \ldots, 50$ (from dark to light hues), safety factor, and normalized mass density.

key to handle the very large number of AEs involved in such systematic stability assessments. Also crucial to this issue is the ability to easily split the workload between several computing units. Indeed, independent tasks can be distributed along $(\omega, \mathbf{k})$-space subsets to be scanned for possible AEs and afterwards along each AE found that needs to have its energy exchange with plasma species evaluated. Such trivially parallelizable workflow enables one to take full advantage of massively-parallel computers.

3 The reference case

The kinetic profiles computed by the transport code `ASTRA` for the ITER $I_\mathrm{p} = 15$ MA baseline scenario [7] are displayed in Figure 1, where $s^2 = \psi/\psi_\mathrm{b}$, ψ is the poloidal flux, and ψ_b is its value at the boundary. Other relevant parameters are the on-axis magnetic field $B_0 = 5.3$ T, the minor radius $a = 2$ m, and the magnetic-axis location at $R_0 = 6.4$ m. The DT fuel mix ratio is $n_\mathrm{D}/n_\mathrm{T} = 1$ and their combined density is $n_\mathrm{i} = n_\mathrm{D} + n_\mathrm{T}$. Peaked temperature profiles contrast with DT-ion and electron density distributions, which are flat almost up to the plasma edge. Conversely, fusion alpha-particles are mostly confined in the core, with the gradient dn_α/ds being almost constant for $0.2 \lesssim s \lesssim 0.6$.

Flat mass-density distributions up to the plasma edge, like the one plotted in Figure 2, contribute to close de frequency gap in the Alfvén continuum arising from the coupling between distinct poloidal harmonics. Consequently, discrete AEs with frequency in such gap can hardly extend towards the plasma boundary without interacting with the Alfvén continuum and therefore sustain significant damping. This property acts as a filter regarding the type of AEs that can be found for the particular plasma state being considered. In fact, the safety-factor profile also depicted in Figure 2 is almost flat in the core region ($s \lesssim 0.5$), yielding well separated gaps for toroidal mode numbers $n \gtrsim 10$. Highly localized low-shear toroidicity-induced AEs (LSTAEs), with only two dominant poloidal harmonics are thus expected to arise in the core. Conversely, on the outer half of the plasma the magnetic shear is higher, gap separation is smaller, and AEs become broader, encompassing a large number of poloidal harmonics and extending to the edge.

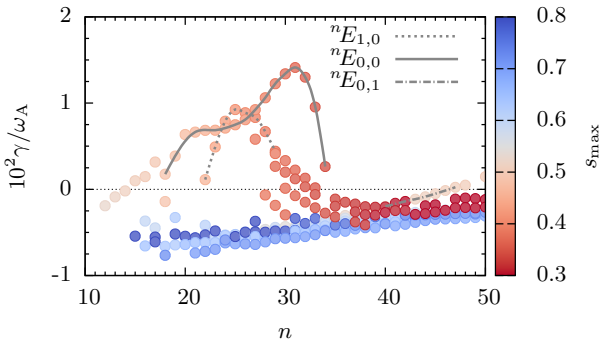

FIG. 3: Distribution of the normalized growth rate by n for I_{ref}, with each AE colored by the radial location of its maximum amplitude. Three AE families are identified by dotted, solid, and dash-dotted lines.

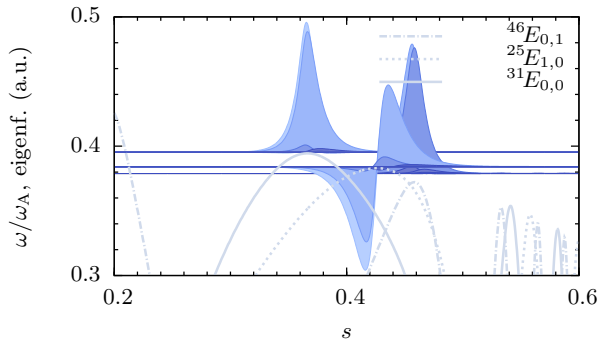

FIG. 4: Example eigenfunctions of the AE families $^nE_{0,1}$, $^nE_{1,0}$, and $^nE_{0,0}$, with baselines at their normalized frequencies (filled curves) and their corresponding ideal Alfvén continuum (light lines).

But in doing so, they interact with the Alfvén continuum and are thus excluded from further analysis, which will be dominated by $n \gtrsim 10$ highly localized LSTAEs.

The $(\omega, \mathbf{k})$-space scan carried out by `MISHKA` finds the radial structure of all AEs with toroidal number n in the range $1 \leqslant n \leqslant 50$ and poloidal harmonics $n - 1 \leqslant m \leqslant n + 15$. The upper limit for n is set by the drift-kinetic ordering in (2) as

$$k_\perp \rho_\alpha \lesssim 1, \quad \text{whence} \quad n \lesssim \big(s/q\big)\big/\big(\rho_\alpha/a\big) \approx 50, \tag{3}$$

with $\rho_\alpha/a \approx 10^{-2}$ the normalized alpha-particle gyro-radius, $k_\perp \approx nq/\big(as\big)$, $q \approx 1$, and $s \approx 0.5$. For each n, the frequency range $0 \leqslant \omega/\omega_A \leqslant 1$ [where $\omega_A = V_A(0)/R_0$ and $V_A(0)$ is the on-axis Alfvén velocity] is sampled in small steps of size 2×10^{-5}. Next, `CASTOR-K` evaluates the energy exchange between every selected AE and each of the three bulk-plasma species (DT ions, electrons, and He ash) and the energetic-particle population. Although other sources of energetic particles are foreseen for the ITER scenario concerned (e.g., 40 MW of combined NBI and ECRH power) [4], only fusion-born alpha-particles are considered in this work. The parameters of their slowing-down distribution in (1) are $E_c = 730$ KeV, $\Delta_E = 50$ KeV, and $E_0 = 3.5$ MeV.

The stability assessment is summarized in Figure 3 for the reference scenario where the plasma current I_p takes the reference value $I_{ref} = 15$ MA and the on-axis safety factor becomes $q_{ref} = 0.987$. This is essentially a subset of previous results [6], here restricted to toroidicity-induced AEs (TAEs) to make the presentation of results clearer. The most unstable modes have $20 \lesssim n \lesssim 30$ and lie in the core ($0.3 \lesssim s \lesssim 0.5$, reddish hues), where dn_α/ds is highest and the magnetic shear is lowest. Conversely, AEs located in the outer half of the plasma (blueish hues) are stable due to small dn_α/ds or interact with the Alfvén continuum, being thus discarded from the analysis.

Three lines are also plotted in Figure 3 connecting AEs belonging to three families that will play a key role in the ensuing discussion. These families are denoted as $^nE_{l,p}$ meaning that their members are LSTAEs with even (E) parity and l zeros, with p being

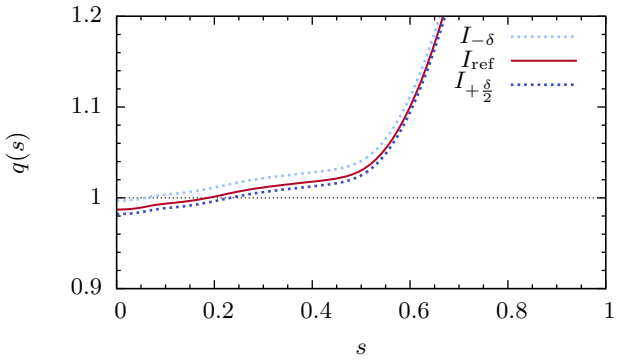

FIG. 5: Safety-factor profiles for three values of I_p.

the difference between the first dominant harmonic m and the toroidal number n. One member of each family is depicted in Figure 4, where they can be identified by their respective Alfvén continuum.

4 Perturbed magnetic equilibria

During ITER operation the plasma-current control system is not exact and so small fluctuations of the plasma current are expected around the value $I_{\rm ref}$. Two different magnetic equilibria are next considered, in addition to the reference one discussed in the previous Section, in order to assess the effects of such fluctuations on the stability properties. These equilibria are obtained changing $I_{\rm p}$ from $I_{\rm ref}$ by the small amounts $-\delta$ and $\delta/2$, with $\delta = 0.16$ MA, whilst keeping the same kinetic profiles. The resulting q profiles are plotted in Figure 5, along with the reference one. As expected, $q(0) \equiv q_0$ changes only slightly by circa 1% and 0.5% respectively, thus following the magnitude of the $I_{\rm p}$ variation from $I_{\rm ref}$. Moreover, the safety-factor derivative in the plasma core is kept almost unchanged in all cases, with $q'(0) \equiv q'_0 \approx 0.07$.

The consequences concerning the stability properties are displayed in Figure 6, where small variations ($\sim 1\%$) in $I_{\rm p}$ or q_0 are seen to cause large changes in the toroidal number ($\sim 20\%$) and normalized growth rate ($\sim 50\%$) of the most unstable AEs. Decreasing $I_{\rm p}$ (and thus raising q_0) pushes the most unstable AE families (${}^nE_{0,0}$ and ${}^nE_{1,0}$) towards lower n and up to larger growth rates. A slight increase in $I_{\rm p}$ yields precisely the opposite. In both cases, the most unstable AEs are still even LSTAEs.

The sensitivity to small changes depicted in Figure 6 can be understood with the aid of the three conditions

$$q(s) = q_0 + q'_0 s, \quad q = 1 + \frac{1}{2n}, \quad \text{and} \quad k_\perp \Delta_{\rm orb} = \left(\frac{nq}{as}\right)\left(\frac{aq}{\varepsilon\tilde{\Omega}}\right) \sim 1. \tag{4}$$

The first one is a radial representation of the safety factor in the low-shear core and the second is a property of the AE family ${}^nE_{l,0}$ regarding the location of its modes resonant surface. In turn, the third relation is a condition for efficient drive, with $\Delta_{\rm orb}$ the alpha-particle orbit width, $\tilde{\Omega} = \Omega_\alpha/\omega_{\rm A}$ its normalized gyro-frequency, and $\varepsilon = a/R_0$ the tokamak

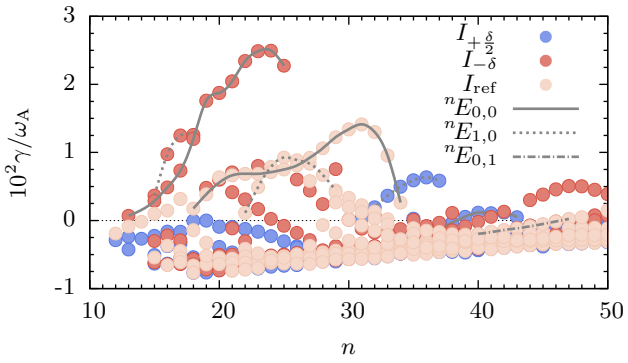

FIG. 6: Distribution of the normalized growth rate by n for three I_p values.

inverse aspect ratio. Together, the three equations in (4) set the three variables s, q, and n corresponding to the most unstable AEs. Solving for the toroidal number, one gets

$$n + \frac{1-2\zeta}{4n} + 1 = \zeta(1-q_0), \tag{5}$$

which is written in terms of the dimensionless number

$$\zeta \equiv \frac{\varepsilon\tilde{\Omega}}{q_0'} = \left(\frac{q}{q_0'}\right)\left(\frac{a}{\Delta_{\rm orb}}\right). \tag{6}$$

Subtracting equation 5 and its evaluation with the values $n_{\rm ref}$ and $q_{\rm ref}$ corresponding to the reference case, gives

$$\left(1 + \frac{2\zeta - 1}{4n_{\rm ref}\, n}\right)\left(n - n_{\rm ref}\right) = -\zeta\left(q_0 - q_{\rm ref}\right), \tag{7}$$

which relates a variation of the on-axis safety factor with a corresponding change in the toroidal number of the most unstable AEs.

ITER parameters are $q_0' \approx 0.07$, $\varepsilon \approx 0.3$, and $\tilde{\Omega} \approx 230$, whence $\zeta \approx 10^3$. On the other hand, $n \sim n_{\rm ref} \sim 30$ and therefore $(2\zeta - 1)/(4n_{\rm ref}n) \sim 1/2$. So, it is the large value attained by ζ that forces small changes of the on-axis safety factor to cause large variations $n - n_{\rm ref}$. Also, one easily checks that increasing q_0 above $q_{\rm ref}$ lowers n below $n_{\rm ref}$ and conversely, as observed in Figure 6. Moreover, the conditions in (4) relate the radial location s of the most unstable AE with its toroidal number as

$$\varepsilon\tilde{\Omega}s = n\left(1 + \frac{1}{2n}\right)^2, \tag{8}$$

which predicts its displacement towards the core as q_0 increases and n drops according to equation (7). In doing so, the AE growth rate rises due to the larger number of alpha-particles found as it moves inwards within $0.2 \lesssim s \lesssim 0.6$, where dn_α/ds is almost constant (Figure 1). The consequences of decreasing q_0 (or raising $I_{\rm p}$) are likewise explained.

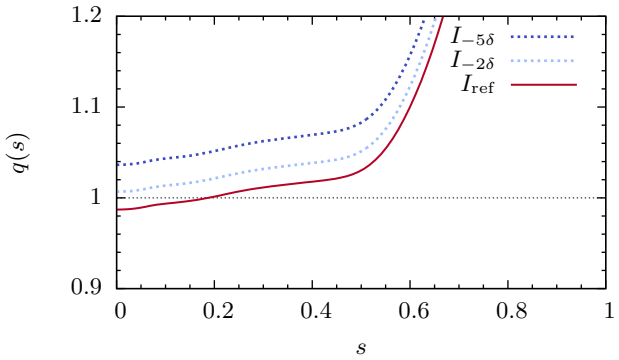

FIG. 7: Safety-factor profiles for three values of I_p.

The contribution of the alpha-particle population to the AEs drive [9]

$$\gamma_\alpha \propto \omega \frac{\partial f_\alpha}{\partial E} - n \frac{\partial f_\alpha}{\partial P_\phi} \tag{9}$$

is proportional to n, with $f_\alpha(E, P_\phi)$ the unperturbed distribution function and P_ϕ the toroidal canonical momentum. Therefore, it may be asked if unstable AEs can be pushed further to lower n by reducing $I_{\rm p}$ and in this way stabilized. To address this question, two additional magnetic equilibria are considered with plasma currents $I_{-2\delta}$ and $I_{-5\delta}$ corresponding, respectively, to reductions of size 2δ and 5δ of the reference value $I_{\rm ref}$. Their safety-factor profiles are plotted in Figure 7 and q_0 increases now by 2% and 5%. As a consequence, the surface $q = 1$ is removed from the plasma and solutions of the AE families ${}^nE_{l,0}$ can exist for low n only.

The new stability assessment is summarized in Figure 8. According to predictions, AE families ${}^nE_{l,0}$ are pushed to lower n and eventually vanish. For $I_{-2\delta}$ and before vanishing, AEs in the family ${}^nE_{0,0}$ have their growth rate reduced by 30% with respect to the reference case. The growth-rate reduction with respect to the case $I_{-\delta}$ is even larger. However, the AE family ${}^nE_{0,1}$ whose resonant surfaces are located at $q = 1 + \frac{3}{2n}$ is also brought to lower n and inwards from its reference radial location. For $I_{-5\delta}$ these AEs are located near the maximum gradient dn_α/ds and their normalized growth rate peaks, accordingly, at 3.2% and $n = 24$. In this way, efforts to stabilize AEs by reducing their n are thwarted by the destabilization of AE families previously stable or weakly unstable.

5 Conclusions

In summary, an hybrid ideal-MHD–drift-kinetic model was shown to efficiently handle routine stability assessments and sensitivity analysis in burning plasmas. The key elements to achieve this aim are code efficiency and the ability to easily share the workload in massive-parallel machines. As an practical application, the stability properties of ITER $I_{\rm p} = 15$ MA baseline scenario were found to be significantly sensitive to eventual small changes in the plasma current or in the on-axis safety factor caused by the plasma-current

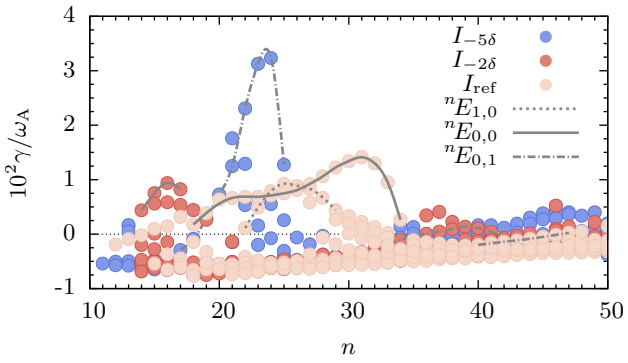

FIG. 8: Distribution of the normalized growth rate by n for three I_p values.

control system. Such small perturbations were seen to cause large changes in the toroidal number and growth rate of the most unstable AEs. Finally, this sensitivity was shown to proceed from the large value attained by the dimensionless parameter ζ, which is caused by the combination of large alpha-particle gyro-frequency with very low magnetic shear in the plasma core.

Acknowledgments

This work was carried out within the framework of the EUROfusion Consortium and received funding from the Euratom research and training programme 2014-2018 under grant agreement no. 633053. IST activities received financial support from "Fundação para a Ciência e Tecnologia" (FCT) through project UID/FIS/50010/2013. The views and opinions expressed herein do not necessarily reflect those of the European Commission, IST, CCFE, or the ITER Organization. All computations were carried out using the HELIOS supercomputer system at the Computational Simulation Centre of the International Fusion Energy Research Centre (IFERC-CSC) in Aomori, Japan, under the Broader Approach collaboration between Euratom and Japan implemented by Fusion for Energy and JAEA. PR was supported by EUROfusion Consortium grant no. WP14-FRF-IST/Rodrigues and NFL was supported by FCT grant no. IF/00530/2013.

References

[1] A. Fasoli *et al.*, Nucl. Fusion **47**, S264 (2007).

[2] B. N. Breizman and S. E. Sharapov, Plasma Phys. Control. Fusion **53**, 054001 (2011).

[3] N. Gorelenkov, S. Pinches, and K. Toi, Nucl. Fusion **54**, 125001 (2014).

[4] S. D. Pinches *et al.*, Phys. Plasmas **22**, 021807 (2015).

[5] P. Lauber, Plasma Phys. Control. Fusion **57**, 054011 (2015).

[6] P. Rodrigues *et al.*, Nucl. Fusion **55**, 083003 (2015).

[7] A. R. Polevoi *et al.*, J. Plasma Fusion Res. SERIES **5**, 82 (2002).

[8] S. Pinches *et al.*, Comp. Phys. Comm. **111**, 133 (1998).

[9] F. Porcelli, R. Stankiewicz, W. Kerner, and H. L. Berk, Phys. Plasmas **1**, 470 (1994).

[10] G. Huysmans, J. Goedbloed, and W. Kerner, Int. J. Mod. Phys. **2**, 371 (1991).

[11] A. B. Mikhailovskii, G. T. A. Huysmans, W. O. K. Kerner, and S. E. Sharapov, Plasma Phys. Rep. **23**, 844 (1997).

[12] D. Borba and W. Kerner, J. Comput. Phys. **153**, 101 (1999).

[13] F. Nabais *et al.*, Plasma Sci. Technol. **17**, 89 (2015).